

Study of $K_0^*(1430)$ and $a_0(980)$ from $B \rightarrow K_0^*(1430)\pi$ and $B \rightarrow a_0(980)K$ Decays

Yue-Long Shen^b, Wei Wang^{b*}, Jin Zhu^b and Cai-Dian Lü^{a,b}

^a CCAST (World Laboratory), P.O. Box 8730, Beijing 100080, P.R. China

^b Institute of High Energy Physics, CAS, P.O.Box 918(4), 100049, P.R. China[†]

We use the decay modes $B \rightarrow K_0^*(1430)\pi$ and $B \rightarrow a_0(980)K$ to study the scalar mesons $K_0^*(1430)$ and $a_0(980)$ within perturbative QCD framework. For $B \rightarrow K_0^*(1430)\pi$, we perform our calculation in two scenarios of the scalar meson spectrum. The results indicate that scenario II is more favored by experimental data than scenario I. The important contribution from annihilation diagrams can enhance the branching ratios about 50% in scenario I, and about 30% in scenario II. The predicted branching ratio of $B \rightarrow a_0(980)K$ in scenario I is also less favored by the experiments. The direct CP asymmetries in $B \rightarrow K_0^*(1430)\pi$ are small, which are consistent with the present experiments.

I. INTRODUCTION

The scalar meson spectrum is an interesting topic for both experimental and theoretical studies, but the underlying structure of the light scalar mesons is still under controversy. Many scalar meson states have been found in experiments: isoscalar states $\sigma(600)$, $f_0(980)$, $f_0(1500)$, $f_0(1370)$, $f_0(1710)$; the isovector states $a_0(980)$, $a_0(1450)$ and isodoublets $\kappa(800)$, $K_0^*(1430)$. In the literature, there are many schemes for the classification of these states [1]. Here are two typical scenarios: the members of the lower mass nonet $\sigma(600)$, $\kappa(800)$, $f_0(980)$, and $a_0(980)$ are treated as the lowest lying $q\bar{q}$ states, while $K_0^*(1430)$ *et al.* which form the higher mass nonet are the first excited $q\bar{q}$ states; In scenario II, the members of the lower mass nonet are treated as the four-quark states [2]. Then the higher mass nonet is considered as the lowest lying $\bar{q}q$ states. There are also other schemes to classify these states, for example, $\sigma(600)$ and $\kappa(800)$ are not considered as the physical states, $a_0(980)$ (or $a_0(1450)$), $f_0(980)$, $K_0^*(1430)$ and $f_0(1500)$ form the $q\bar{q}$ nonet [3]. In this paper, we study the scalar mesons in the first two scenarios.

Although intensive study has been given to the decay property of the scalar mesons, the production of these mesons can provide a different unique insight to the mysterious structure of these mesons. Compared with D meson decays, the phase space in B decays is larger, thus B decays can provide a better place to study the scalar resonances. Experimentally, B meson decay channels with a final state scalar meson have been measured in B factories for several years [4]. Much more measurements have been reported by BABAR and Belle [5, 6, 7, 8, 9] recently (see [10] for more experimental data). On the theoretical side, the B decays which involve a scalar meson have been systematically studied using QCD factorization (QCDF) approach by Cheng, Chua and Yang [11]. They draw the conclusion that scenario II is more preferable. For example, in scenario I, the predicted branching ratio of $B^- \rightarrow \bar{K}_0^* \pi^-$ without annihilation is only about 1×10^{-5} , which is much smaller than the experimental results. In order to explain the large data, the annihilation contribution is required to be large. But in this scenario, $a_0(980)$ is also a $q\bar{q}$ state and the $SU(3)$ symmetry implies a much large annihilation contribution to $B \rightarrow a_0(980)K$. This large annihilation contribution can lead to a larger branching ratio than the experimental upper bound. Then it is concluded that scenario I is less preferable than scenario II.

The annihilation topology contribution plays such an important role that we should pay much more attention to it. In QCD factorization approach, which is based on collinear factorization, the so-called endpoint singularity makes the annihilation contribution divergent. This might be resolved by applying the “zero-bin” subtractions which will lead to

* Email:wwang@mail.ihep.ac.cn

† Mailing address

new factorization theorems in rapidity space [12]. The more popular way to handle this divergence is the Perturbative QCD (PQCD) approach [13, 14]. Using this approach, some pure annihilation type decays have been studied and the results are consistent with the experiments [15], which indicates it a reliable method to deal with annihilation diagrams. In the present paper, we will use the PQCD approach to calculate the decay modes $B \rightarrow K_0^*(1430)\pi$ and $B \rightarrow a_0(980)K$ (in the following, we use K_0^* and a_0 to denote $K_0^*(1430)$ and $a_0(980)$ for convenience). We will examine how large the annihilation topology contribution is, and find whether there are enough reasons to determine which scenario is more appropriate through these decay channels.

This paper is organized as follows: in the next section, we give a brief review of the scalar meson wave functions, which are important inputs in PQCD approach. What followed is the analysis of the $B \rightarrow K_0^*\pi$ and $B \rightarrow a_0K$ decays. The numerical results and the discussions are given in the section IV. Our conclusions are presented in the final part.

II. SCALAR MESON DISTRIBUTION AMPLITUDES

In the two-quark picture, the decay constants f_S and \bar{f}_S for a scalar meson S are defined by:

$$\langle S(p)|\bar{q}_2\gamma_\mu q_1|0\rangle = f_S p_\mu, \quad \langle S(p)|\bar{q}_2 q_1|0\rangle = \bar{f}_S m_S, \quad (1)$$

where $m_S(p)$ is the mass (momentum) of the scalar meson. The vector current decay constant f_S is zero for neutral scalar mesons σ , f_0 and a_0^0 due to the charge conjugation invariance or G parity conservation. In the $SU(3)$ limit, the vector decay constant of K_0^* also vanishes. After including the $SU(3)$ symmetry breaking, it only gets a very small value which is proportional to the mass difference of the constituent quarks. The scalar density decay constant \bar{f}_S can be related to the vector one by the equation of motion:

$$\mu_S f_S = \bar{f}_S, \quad (2)$$

where μ_S is defined by $\mu_S = \frac{m_S}{m_{q_2}(\mu) - m_{q_1}(\mu)}$, which is scale dependent, thus the scalar decay constant is also scale dependent. Many model calculations have been performed for the K_0^* and a_0 [16]. In this paper we will use the values from QCD sum rules in ref. [11]. Fixing the scale at 1GeV, we specify them below:

$$\begin{aligned} \text{scenario I: } \quad \bar{f}_{K_0^*} &= -(300 \pm 30)\text{MeV}, \quad f_{K_0^*} = -(25 \pm 2)\text{MeV}, \\ \bar{f}_{a_0} &= (365 \pm 20)\text{MeV}; \end{aligned} \quad (3)$$

$$\text{scenario II: } \quad \bar{f}_{K_0^*} = (445 \pm 50)\text{MeV}, \quad f_{K_0^*} = (37 \pm 4)\text{MeV}. \quad (4)$$

Now we turn to the distribution amplitudes. The scalar meson's light-cone distribution amplitude is defined by:

$$\begin{aligned} \langle S(p)|\bar{q}_{1\beta}(z)q_{2\alpha}(0)|0\rangle &= \frac{1}{\sqrt{6}} \int_0^1 dx e^{ixp \cdot z} \left\{ \not{p}\phi_S(x) + m_S\phi_S^S(x) - \frac{1}{6}m_S\sigma_{\mu\nu}p^\mu z^\nu\phi_S^\sigma(x) \right\}_{\alpha\beta} \\ &= \frac{1}{\sqrt{6}} \int_0^1 dx e^{ixp \cdot z} \left\{ \not{p}\phi_S(x) + m_S\phi_S^S(x) + \frac{1}{6}m_S(\not{n}\not{\bar{n}} - 1)\phi_S^T(x) \right\}_{\alpha\beta}, \end{aligned} \quad (5)$$

where $n = (1, 0, 0_T)$ and $\bar{n} = (0, 1, 0_T)$ are dimensionless vectors on the light cone, and n is parallel with the moving direction of the scalar meson. The distribution amplitudes $\phi_S(x)$, $\phi_S^S(x)$ and $\phi_S^\sigma(x)$ are normalized as:

$$\int_0^1 dx \phi_S(x) = \frac{f_S}{2\sqrt{6}}, \quad \int_0^1 dx \phi_S^S(x) = \int_0^1 dx \phi_S^\sigma(x) = \frac{\bar{f}_S}{2\sqrt{6}}, \quad (6)$$

and $\phi_S^T(x) = \frac{d}{dx}\phi_S^\sigma(x)$.

In general, the twist-2 light cone distribution amplitude $\phi_S(x)$ can be expanded as:

$$\begin{aligned}\phi_S(x, \mu) &= \frac{\bar{f}_S(\mu)}{2\sqrt{6}} 6x(1-x) \left[B_0(\mu) + \sum_{m=1}^{\infty} B_m(\mu) C_m^{3/2}(2x-1) \right] \\ &= \frac{f_S(\mu)}{2\sqrt{6}} 6x(1-x) \left[1 + \mu_S \sum_{m=1}^{\infty} B_m(\mu) C_m^{3/2}(2x-1) \right],\end{aligned}\quad (7)$$

where $B_m(\mu)$ and $C_m^{3/2}(x)$ are the Gegenbauer moments and Gegenbauer polynomials respectively. The Gegenbauer moments B_1, B_3 of distribution amplitudes for K_0^* and a_0 have been calculated in [11] as

$$\text{scenario I: } B_1 = 0.58 \pm 0.07, \quad B_3 = -1.20 \pm 0.08; \quad (8)$$

$$B_1 = -0.93 \pm 0.10, \quad B_3 = 0.14 \pm 0.08; \quad (9)$$

$$\text{scenario II: } B_1 = -0.57 \pm 0.13, \quad B_3 = -0.42 \pm 0.22, \quad (10)$$

where the second line is for a_0 , and the others are for K_0^* . These values are also taken at $\mu = 1\text{GeV}$.

As for the twist-3 light-cone distribution amplitudes, there is no study on their explicit Gegenbauer moments so far, so we take the asymptotic form in our numerical calculation:

$$\phi_S^S(x) = \bar{f}_S, \quad \phi_S^T(x) = 6\bar{f}_S(1-2x). \quad (11)$$

In our calculation, we will choose the momentum fraction on the anti-quark, thus we should use $\phi_S(1-x)$, $\phi_S^S(1-x) = \phi^S(x)$ and $\phi_S^T(1-x) = -\phi_S^T(x)$. But in the amplitudes, for simplicity, we use $\phi_S(x)$ to denote $\phi_S(1-x)$. It is similar for the pseudoscalar meson.

III. THE PERTURBATIVE QCD CALCULATION

In this section we will give the decay amplitudes for the $B \rightarrow K_0^* \pi$ and $B \rightarrow a_0 K$ decays in the PQCD approach. The PQCD approach is based on the k_T factorization [17], where we keep the transverse momentum of the partons in a meson. In this approach there is no divergence when the longitudinal parton momentum fraction falls into the endpoint region. The weak decay matrix element can be completely factorized [18]:

$$\mathcal{A} = \phi_B \otimes H^{(6)} \otimes J \otimes S \otimes \phi_{M_1} \otimes \phi_{M_2}, \quad (12)$$

where ϕ_B , ϕ_{M_1} and ϕ_{M_2} denote the wave functions of the B meson and the light mesons, respectively. S and J denote the Sudakov form factor and the jet function respectively. The Sudakov form factor comes from k_T resummation which kills the end-point singularities. The jet function is from threshold resummation which can organize the large double logarithms in the hard kernel. The symbol \otimes denotes convolution of the parton longitudinal momentum fractions and the transverse momentum. $H^{(6)}$ is the six-quark hard scattering kernel, which consists of the effective four quark operators and a hard gluon to connect the spectator quark in the decay. The standard four-quark operators describing the $b \rightarrow s$ transition are defined as [19]:

- current-current tree operators

$$O_1 = (\bar{u}_\alpha b_\beta)_{V-A} (\bar{s}_\beta u_\alpha)_{V-A}, \quad O_2 = (\bar{u}_\alpha b_\alpha)_{V-A} (\bar{s}_\beta u_\beta)_{V-A}, \quad (13)$$

- QCD penguin operators

$$O_3 = (\bar{s}_\alpha b_\alpha)_{V-A} \sum_{q'} (\bar{q}'_\beta q'_\beta)_{V-A}, \quad O_4 = (\bar{s}_\beta b_\alpha)_{V-A} \sum_{q'} (\bar{q}'_\alpha q'_\beta)_{V-A}, \quad (14)$$

$$O_5 = (\bar{s}_\alpha b_\alpha)_{V-A} \sum_{q'} (\bar{q}'_\beta q'_\beta)_{V+A}, \quad O_6 = (\bar{s}_\beta b_\alpha)_{V-A} \sum_{q'} (\bar{q}'_\alpha q'_\beta)_{V+A}, \quad (15)$$

- electro-weak penguin operators

$$O_7 = \frac{3}{2}(\bar{s}_\alpha b_\alpha)_{V-A} \sum_{q'} e_{q'}(\bar{q}'_\beta q'_\beta)_{V+A}, \quad O_8 = \frac{3}{2}(\bar{s}_\beta b_\alpha)_{V-A} \sum_{q'} e_{q'}(\bar{q}'_\alpha q'_\beta)_{V+A}, \quad (16)$$

$$O_9 = \frac{3}{2}(\bar{s}_\alpha b_\alpha)_{V-A} \sum_{q'} e_{q'}(\bar{q}'_\beta q'_\beta)_{V-A}, \quad O_{10} = \frac{3}{2}(\bar{s}_\beta b_\alpha)_{V-A} \sum_{q'} e_{q'}(\bar{q}'_\alpha q'_\beta)_{V-A}, \quad (17)$$

where $q' = (u, d, s, c, b)$. The 10 operators together with their QCD-corrected Wilson coefficients form the effective Hamiltonian:

$$\mathcal{H}_{eff} = \frac{G_F}{\sqrt{2}} \left\{ V_{ub}V_{us}^* \left[C_1(\mu)O_1(\mu) + C_2(\mu)O_2(\mu) \right] - V_{tb}V_{ts}^* \sum_{i=3}^{10} C_i(\mu)O_i(\mu) \right\}. \quad (18)$$

The partition of the perturbative and non-perturbative region (factorization scale) is quite arbitrary, but the full amplitude should be independent of the partition. We usually take the largest virtuality of internal particles as the factorization scale, which is of order $\sqrt{m_B\Lambda}$. The leading order Wilson coefficients will be evolved to this scale. As the factorization scale in PQCD approach is smaller than the factorization scale of QCDF, which is about m_B , a large enhancement of the Wilson coefficients occurs, especially for the penguin operators [13, 14].

A. $B \rightarrow K_0^* \pi$ decays

The leading order Feynman diagrams for these decays in PQCD approach are given in Fig. 1. The decay amplitude for each diagram can be obtained by contracting the hard scattering kernels and the meson's wave functions. According to the power counting in PQCD approach [20], the first two emission diagrams in Fig. 1 give the dominant contribution. For the $(V-A)(V-A)$ kind of operators, the decay amplitudes for these two diagrams are given by:

$$\begin{aligned} F_{B \rightarrow \pi}^L(a) = & \frac{32\pi}{3} m_B^4 f_{K_0^*} \int_0^1 dx_1 dx_3 \int_0^\infty b_1 db_1 b_3 db_3 \phi_B(x_1, b_1) \left\{ a(t) E_e(t) \right. \\ & \times \left[(1+x_3)\phi_\pi^A(x_3) + r_\pi(1-2x_3)(\phi_\pi^P(x_3) + \phi_\pi^T(x_3)) \right] h_e(x_1, x_3, b_1, b_3) \\ & \left. + 2r_\pi \phi_\pi^P(x_3) a(t') E_e(t') h_e(x_3, x_1, b_3, b_1) \right\}, \end{aligned} \quad (19)$$

where $r_\pi = m_0^\pi/m_B$, m_0^π is the chiral enhancement scale and a is the corresponding Wilson coefficient. $E_e(t)$ is defined as

$$E_e(t) = \alpha_s(t) \exp[-S_B(t) - S_\pi(t)]. \quad (20)$$

For the $(V-A)(V+A)$ kind of operators, the decay amplitudes for these two diagrams are given by:

$$\begin{aligned} F_{B \rightarrow \pi}^R(a) = & -\frac{64\pi}{3} m_B^4 r_{K_0^*} \overline{f_{K_0^*}} \int_0^1 dx_1 dx_3 \int_0^\infty b_1 db_1 b_3 db_3 \phi_B(x_1, b_1) \left\{ a(t) E_e(t) \right. \\ & \times \left[\phi_\pi^A(x_3) + r_\pi x_3 (\phi_\pi^P(x_3) - \phi_\pi^T(x_3)) + 2r_\pi \phi_\pi^P(x_2) \right] h_e(x_1, x_3, b_1, b_3) \\ & \left. + 2r_\pi \phi_2^P(x_3) a(t') E_e(t') h_e(x_3, x_1, b_3, b_1) \right\}, \end{aligned} \quad (21)$$

with the factorization scales $t = \max\{\sqrt{x_3}m_B, 1/b_1, 1/b_3\}$ and $t' = \max\{\sqrt{x_1}m_B, 1/b_1, 1/b_3\}$, $r_{K_0^*} = m_{K_0^*}/m_B$. The Sudakov form factors $S_B(t)$ and $S_\pi(t)$ and the hard functions h_e and others like h_a , h_{na} are given explicitly in ref.[13, 14].

Comparing $F_{B \rightarrow \pi}^L$ and $F_{B \rightarrow \pi}^R$, we find that the first one is proportional to the small vector decay constant, but the latter is proportional to the scalar decay constant which is strongly chiral enhanced, so $F_{B \rightarrow \pi}^R$ will give the dominant contribution.

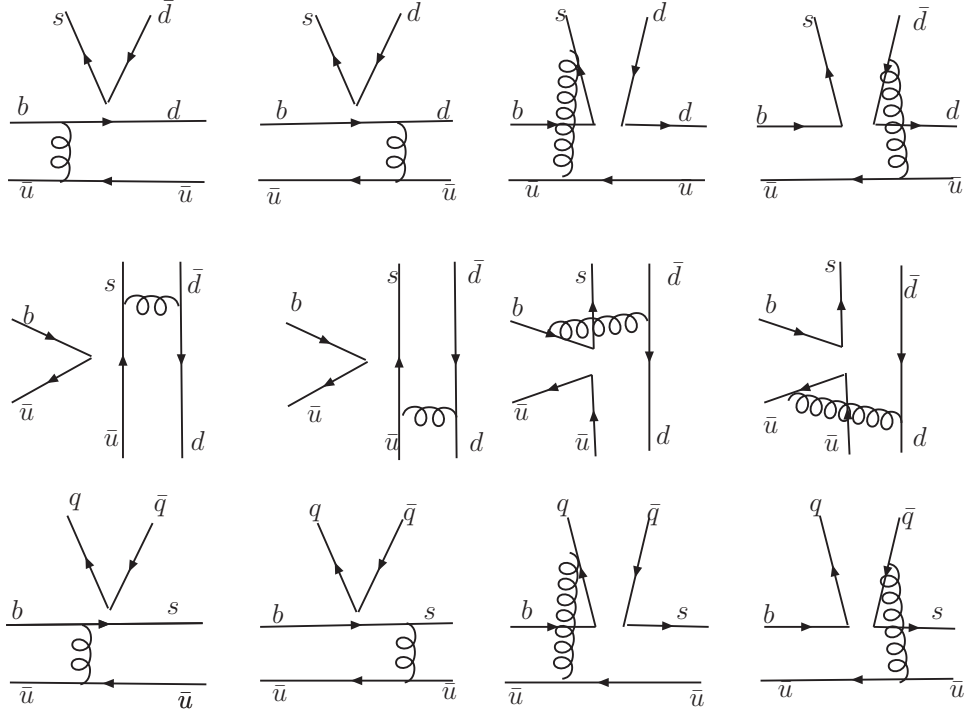


FIG. 1: The leading order Feynman diagrams in PQCD for $B \rightarrow K_0^* \pi$ and $B \rightarrow a_0 K$

In ref. [11], the author found that the vertex corrections and hard-spectator-scattering corrections can enhance a_4 sizably. In PQCD approach, the vertex corrections are at the next-to-leading order in α_s , so we neglect it in our calculation, but we include the hard spectator scattering (the last two diagrams in the first row of Fig. 1). After the calculation, the non-factorization decay amplitudes for the $(V - A)(V - A)$ kind of operators read:

$$\begin{aligned}
 \mathcal{M}_{B \rightarrow \pi}^L(a) &= \frac{128\pi}{3\sqrt{6}} m_B^4 \int_0^1 dx_1 dx_2 dx_3 \int_0^\infty b_1 db_1 b_2 db_2 \phi_B(x_1, b_1) \phi_{K_0^*}(x_2) \\
 &\times \left\{ - \left[(x_2 - 1) \phi_\pi(x_3) + r_\pi x_3 (\phi_\pi^P(x_3) - \phi_\pi^T(x_3)) \right] a(t) E'_e(t) h_n(x_1, 1 - x_2, x_3, b_1, b_2) \right. \\
 &\left. - \left[(x_2 + x_3) \phi_\pi(x_3) - r_\pi x_3 (\phi_\pi^P(x_3) + \phi_\pi^T(x_3)) \right] a(t') E'_e(t') h_n(x_1, x_2, x_3, b_1, b_2) \right\}. \quad (22)
 \end{aligned}$$

For the $(V - A)(V + A)$ kind of operators, the decay amplitudes for these two diagrams are given by:

$$\begin{aligned}
 \mathcal{M}_{B \rightarrow \pi}^R(a) &= \frac{128\pi}{3\sqrt{6}} m_B^4 r_{K_0^*} \int_0^1 dx_1 dx_2 dx_3 \int_0^\infty b_1 db_1 b_2 db_2 \phi_B(x_1, b_1) \left\{ a(t) E'_e(t) \times \right. \\
 &\left[(x_2 - 1) (\phi_\pi^A(x_3) (\phi_{K_0^*}^S(x_2) + \phi_{K_0^*}^T(x_2)) + r_\pi (\phi_\pi^P(x_3) - \phi_\pi^T(x_3)) (\phi_{K_0^*}^S(x_2) + \phi_{K_0^*}^T(x_2))) \right. \\
 &\quad \left. - r_\pi x_3 (\phi_\pi^P(x_3) + \phi_\pi^T(x_3)) (\phi_{K_0^*}^S(x_2) - \phi_{K_0^*}^T(x_2)) \right] h_n(x_1, 1 - x_2, x_3, b_1, b_2) + \\
 &\left[x_2 \phi_\pi^A(x_3) (\phi_{K_0^*}^S(x_2) - \phi_{K_0^*}^T(x_2)) + r_\pi x_2 (\phi_\pi^P(x_3) - \phi_\pi^T(x_3)) (\phi_{K_0^*}^S(x_2) - \phi_{K_0^*}^T(x_2)) \right. \\
 &\quad \left. + r_\pi x_3 (\phi_\pi^P(x_3) + \phi_\pi^T(x_3)) (\phi_{K_0^*}^S(x_2) + \phi_{K_0^*}^T(x_2)) \right] a(t') E'_e(t') h_n(x_1, x_2, x_3, b_1, b_2) \left. \right\}, \quad (23)
 \end{aligned}$$

where $E'_e(t) = \alpha_s(t) \exp[-S_B(t) - S_2(t) - S_3(t)]$, the factorization scales are chosen by

$$t = \max\{\sqrt{x_1 x_3} m_B, \sqrt{|(1-x_1-x_2)x_3|} m_B, 1/b_1, 1/b_2\}, \quad (24)$$

$$t' = \max\{\sqrt{x_1 x_3} m_B, \sqrt{|(x_1-x_2)x_3|} m_B, 1/b_1, 1/b_2\}. \quad (25)$$

From the above formulae, we can see that the two hard spectator scattering diagrams contribute constructively for $\mathcal{M}_{B \rightarrow \pi}^L$ while most contributions cancelled for $\mathcal{M}_{B \rightarrow \pi}^R$. So it is expected that the $(V-A)(V-A)$ kind operator contribution can give an important contribution as in $B \rightarrow f_0 K$ [21]. However, these diagrams are suppressed compared with the factorizable ones for a smaller Wilson coefficient C_3 , thus they cannot play such an important role as in QCDF [11].

In PQCD approach, the annihilation type diagrams are free of endpoint singularity, so they can be calculated systematically. The Feynman diagrams are plotted in the second row of Fig. 1. For the first two factorizable annihilation diagrams, the decay amplitude formulae are written as:

$$\begin{aligned} F_a^L(a) = & \frac{32\pi}{3} m_B^4 f_B \int_0^1 dx_2 dx_3 \int_0^\infty b_2 db_2 b_3 db_3 \\ & \times \left\{ \left[(x_3 - 1) \phi_\pi^A(x_3) \phi_{K_0^*}^S(x_2) - 2r_\pi r_{K_0^*} (x_3 - 2) \phi_\pi^P(x_3) \phi_{K_0^*}^S(x_2) \right. \right. \\ & \quad \left. \left. + 2r_\pi r_{K_0^*} x_3 \phi_{K_0^*}^S(x_2) \phi_\pi^T(x_3) \right] a(t) E_a(t) h_a(x_2, 1 - x_3, b_2, b_3) \right. \\ & \left. + \left[x_2 \phi_\pi^A(x_3) \phi_{K_0^*}^S(x_2) - 2r_\pi r_{K_0^*} \phi_\pi^P(x_3) ((x_2 + 1) \phi_{K_0^*}^S(x_2) + (x_2 - 1) \phi_{K_0^*}^T(x_2)) \right] \right. \\ & \left. \times a(t') E_a(t') h_a(1 - x_3, x_2, b_3, b_2) \right\}, \quad (26) \end{aligned}$$

for the $(V-A)(V-A)$ kind of operators and

$$\begin{aligned} F_a^R(a) = & -\frac{64\pi}{3} m_B^4 f_B \int_0^1 dx_2 dx_3 \int_0^\infty b_2 db_2 b_3 db_3 \left\{ E_a(t) a(t) h_a(x_2, 1 - x_3, b_2, b_3) \right. \\ & \times \left[r_\pi (x_3 - 1) \phi_{K_0^*}^S(x_2) (\phi_\pi^P(x_3) + \phi_\pi^T(x_3)) + 2r_{K_0^*} \phi_\pi(x_3) \phi_{K_0^*}^S(x_2) \right] \\ & - \left[2r_\pi \phi_{K_0^*}^S(x_2) \phi_\pi^P(x_3) + r_{K_0^*} x_2 \phi_\pi(x_3) (\phi_{K_0^*}^T(x_2) - \phi_{K_0^*}^S(x_2)) \right] \\ & \left. \times a(t') E_a(t') h_a(1 - x_3, x_2, b_3, b_2) \right\}, \quad (27) \end{aligned}$$

for the $(V-A)(V+A)$ kind of operators, where

$$E_a(t) = \alpha_s(t) \exp[-S_2(t) - S_3(t)], \quad (28)$$

with $t = \max\{\sqrt{1-x_3} m_B, 1/b_2, 1/b_3\}$ and $t' = \max\{\sqrt{x_2} m_B, 1/b_2, 1/b_3\}$.

For the non-factorizable annihilation diagrams, e.g., the last two diagrams in the second row of Fig. 1, the factorization formulae read:

$$\begin{aligned} \mathcal{M}_a^L(a) = & \frac{128\pi}{3\sqrt{6}} m_B^4 \int_0^1 dx_1 dx_2 dx_3 \int_0^\infty b_1 db_1 b_2 db_2 \phi_B(x_1, b_1) \left\{ [-x_2 \phi_\pi^A(x_3) \phi_{K_0^*}^S(x_2) \right. \\ & \quad \left. + r_\pi r_{K_0^*} \phi_\pi^P(x_3) ((x_2 - x_3 + 3) \phi_{K_0^*}^S(x_2) + (x_2 + x_3 - 1) \phi_{K_0^*}^T(x_2)) \right. \\ & \quad \left. + r_\pi r_{K_0^*} \phi_\pi^T(x_3) ((1 - x_2 - x_3) \phi_{K_0^*}^S(x_2) + (1 - x_2 + x_3) \phi_{K_0^*}^T(x_2)) \right] \\ & \times a(t) E'_e(t) h_{na}(x_1, x_2, x_3, b_1, b_2) - [(x_3 - 1) \phi_\pi^A(x_3) \phi_{K_0^*}^S(x_2) \\ & \quad \left. + r_\pi r_{K_0^*} \phi_\pi^P(x_3) ((x_2 - x_3 + 1) \phi_{K_0^*}^S(x_2) - (x_2 + x_3 - 1) \phi_{K_0^*}^T(x_2)) \right] \end{aligned}$$

$$\begin{aligned}
& + r_\pi r_{K_0^*} \phi_\pi^T(x_3) \left[(x_2 + x_3 - 1) \phi_{K_0^*}^S(x_2) - (1 + x_2 - x_3) \phi_{K_0^*}^T(x_2) \right] \\
& \times a(t') E_e'(t') h'_{na}(x_1, x_2, x_3, b_1, b_2) \Big\} ,
\end{aligned} \tag{29}$$

and for the $(V - A)(V - A)$ kind of operators

$$\begin{aligned}
\mathcal{M}_a^R(a) &= \frac{128\pi}{3\sqrt{6}} m_B^4 \int_0^1 dx_1 dx_2 dx_3 \int_0^\infty b_1 db_1 b_2 db_2 \phi_B(x_1, b_1) \times \\
& \left\{ \left[r_\pi(x_3 - 1) \phi_{K_0^*}(x_2) (\phi_\pi^T(x_3) - \phi_\pi^P(x_3)) + r_{K_0^*} x_2 \phi_\pi(x_3) (\phi_{K_0^*}^S(x_2) + \phi_{K_0^*}^T(x_2)) \right] \right. \\
& \times a(t) E_e'(t) h_{na}(x_1, x_2, x_3, b_1, b_2) \\
& - \left[r_\pi(x_3 - 1) \phi_{K_0^*}(x_2) (\phi_\pi^T(x_3) - \phi_\pi^P(x_3)) + r_{K_0^*} x_2 \phi_\pi(x_3) (\phi_{K_0^*}^S(x_2) + \phi_{K_0^*}^T(x_2)) \right] \\
& \left. \times a(t') E_e'(t') h'_{na}(x_1, x_2, x_3, b_1, b_2) \right\} ,
\end{aligned} \tag{30}$$

for the $(V - A)(V + A)$ kind of operators, where

$$\begin{aligned}
t &= \max \{ \sqrt{x_2(1-x_3)} m_B, \sqrt{1 - (1-x_1-x_2)x_3} m_B, 1/b_1, 1/b_2 \}, \\
t' &= \max \{ \sqrt{x_2(1-x_3)} m_B, \sqrt{|(x_1-x_2)(1-x_3)|} m_B, 1/b_1, 1/b_2 \}.
\end{aligned}$$

Summing up all contributions mentioned above, the decay amplitude for $B \rightarrow \overline{K_0^*} \pi^-$ is

$$\begin{aligned}
A(B^- \rightarrow \overline{K_0^*} \pi^-) &= \frac{G_F}{\sqrt{2}} \left[V_{ub} V_{us}^* \left\{ F_a^L(a_1) + \mathcal{M}_a^L(C_1) \right\} \right. \\
& - V_{tb} V_{ts}^* \left\{ F_e^L(a_4 - \frac{1}{2}a_{10}) + F_e^R(a_6 - \frac{1}{2}a_8) + F_a^L(a_4 + a_{10}) + F_a^R(a_6 + a_8) \right. \\
& \left. \left. + \mathcal{M}_e^L(C_3 - \frac{1}{2}C_9) + \mathcal{M}_e^R(C_5 - \frac{1}{2}C_7) + \mathcal{M}_a^L(C_3 - \frac{1}{2}C_9) + \mathcal{M}_a^R(C_5 - \frac{1}{2}C_7) \right\} \right] ,
\end{aligned} \tag{31}$$

where the combinations of Wilson coefficients are defined as usual [22]:

$$a_1 = C_2 + C_1/3, \quad a_3 = C_3 + C_4/3, \quad a_5 = C_5 + C_6/3, \quad a_7 = C_7 + C_8/3, \quad a_9 = C_9 + C_{10}/3, \tag{32}$$

$$a_2 = C_1 + C_2/3, \quad a_4 = C_4 + C_3/3, \quad a_6 = C_6 + C_5/3, \quad a_8 = C_8 + C_7/3, \quad a_{10} = C_{10} + C_9/3. \tag{33}$$

For the decays $\overline{B}^0 \rightarrow K_0^{*-} \pi^+$, $B^- \rightarrow K_0^{*-} \pi^0$ and $\overline{B}^0 \rightarrow \overline{K_0^*} \pi^0$, the analysis is similar, except the last two channels include the π -emission diagrams in the third row of Fig. 1. The decay amplitudes of the factorizable π -emission diagrams for the $(V - A)(V - A)$ kind of operators are written by:

$$\begin{aligned}
F_{B \rightarrow K_0^*}^L(a) &= \frac{32\pi}{3} m_B^4 f_\pi \int_0^1 dx_1 dx_2 \int_0^\infty b_1 db_1 b_2 db_2 \phi_B(x_1, b_1) \left\{ a(t) E_e(t) \right. \\
& \times \left[(1 + x_2) \phi_{K_0^*}(x_2) - r_{K_0^*} (1 - 2x_2) \left(\phi_{K_0^*}^S(x_2) + \phi_{K_0^*}^T(x_2) \right) \right] h_e(x_1, x_2, b_1, b_2) \\
& \left. - 2r_{K_0^*} \phi_{K_0^*}^S(x_2) a(t') E_e(t') h_e(x_2, x_1, b_2, b_1) \right\} ,
\end{aligned} \tag{34}$$

and for the $(V - A)(V + A)$ kind of operators:

$$F_{B \rightarrow K_0^*}^R(a) = -F_{B \rightarrow K_0^*}^L(a). \tag{35}$$

For the non-factorizable diagrams $(V - A)(V - A)$ operators:

$$\mathcal{M}_{B \rightarrow K_0^*}^L(a) = \frac{128\pi}{3\sqrt{6}} m_B^4 \int_0^1 dx_1 dx_2 dx_3 \int_0^\infty b_1 db_1 b_3 db_3 \phi_B(x_1, b_1) \phi_\pi^A(x_3) \left\{ a(t) E_e'(t) \right.$$

$$\begin{aligned}
& \left[(1-x_3)\phi_{K_0^*}(x_2) + r_{K_0^*}x_2 \left(\phi_{K_0^*}^s(x_2) - \phi_{K_0^*}^T(x_2) \right) \right] h_n(x_1, 1-x_3, x_2, b_1, b_3) \\
& + \left[-(x_2+x_3)\phi_{K_0^*}(x_2) - r_{K_0^*}x_2(\phi_{K_0^*}^s(x_2) + \phi_{K_0^*}^T(x_2)) \right] \\
& a(t')E_e'(t')h_n(x_1, x_3, x_2, b_1, b_3) \Big\}, \tag{36}
\end{aligned}$$

and for $(V-A)(V+A)$ operators

$$\begin{aligned}
\mathcal{M}_{B \rightarrow K_0^*}^R(a) &= \frac{128\pi}{3\sqrt{6}} m_B^4 \int_0^1 dx_1 dx_2 dx_3 \int_0^\infty b_1 db_1 b_3 db_3 \phi_B(x_1, b_1) \phi_\pi^A(x_3) \Big\{ -a(t)E_e'(t) \\
& \left[(x_2-x_3+1)\phi_{K_0^*}(x_2) + r_{K_0^*}x_2(\phi_{K_0^*}^s(x_2) + \phi_{K_0^*}^T(x_2)) \right] h_n(x_1, 1-x_3, x_2, b_1, b_3) \\
& + \left[x_3\phi_{K_0^*}(x_2) + r_{K_0^*}x_2(\phi_{K_0^*}^s(x_2) - \phi_{K_0^*}^T(x_2)) \right] a(t')E_e'(t')h_n(x_1, x_3, x_2, b_1, b_3) \Big\}. \tag{37}
\end{aligned}$$

We write the decay amplitudes for the other three channels below:

$$\begin{aligned}
A(\bar{B}^0 \rightarrow K_0^{*-}\pi^+) &= \frac{G_F}{\sqrt{2}} \left[V_{ub}V_{us}^* \left\{ F_{B \rightarrow \pi}^L(a_1) + \mathcal{M}_{B \rightarrow \pi}^L(C_1) \right\} \right. \\
& - V_{tb}V_{ts}^* \left\{ F_{B \rightarrow \pi}^L(a_4 + a_{10}) + F_{B \rightarrow \pi}^R(a_6 + a_8) + F_a^L(a_4 - \frac{1}{2}a_{10}) + F_a^R(a_6 - \frac{1}{2}a_8) \right. \\
& \left. \left. + \mathcal{M}_{B \rightarrow \pi}^L(C_3 + C_9) + \mathcal{M}_{B \rightarrow \pi}^R(C_5 + C_7) + \mathcal{M}_a^L(C_3 - \frac{1}{2}C_9) + \mathcal{M}_a^R(C_5 - \frac{1}{2}C_7) \right\} \right], \tag{38}
\end{aligned}$$

$$\begin{aligned}
A(B^- \rightarrow K_0^{*-}\pi^0) &= \frac{G_F}{2} \left[V_{ub}V_{us}^* \left\{ F_{B \rightarrow \pi}^L(a_1) + \mathcal{M}_{B \rightarrow \pi}^L(C_1) + F_{B \rightarrow K_0^*}^L(a_2) + \mathcal{M}_{B \rightarrow K_0^*}^L(C_2) + F_a^L(a_1) + \mathcal{M}_a^L(C_1) \right\} \right. \\
& - V_{tb}V_{ts}^* \left\{ F_{B \rightarrow \pi}^L(a_4 + a_{10}) + F_{B \rightarrow \pi}^R(a_6 + a_8) + F_{B \rightarrow K_0^*}^L(\frac{3}{2}a_9 - \frac{3}{2}a_7) \right. \\
& + F_a^L(a_4 + a_{10}) + F_a^R(a_6 + a_8) \\
& + \mathcal{M}_{B \rightarrow \pi}^L(C_3 + C_9) + \mathcal{M}_{B \rightarrow \pi}^R(C_5 + C_7) + \mathcal{M}_{B \rightarrow K_0^*}^L(\frac{3}{2}C_{10}) + \mathcal{M}_{B \rightarrow K_0^*}^R(\frac{3}{2}C_8) \\
& \left. \left. + \mathcal{M}_a^L(C_3 + C_{10}) + \mathcal{M}_a^R(C_5 + C_7) \right\} \right], \tag{39}
\end{aligned}$$

$$\begin{aligned}
A(\bar{B}^0 \rightarrow \bar{K}_0^{*0}\pi^0) &= \frac{G_F}{2} \left[V_{ub}V_{us}^* \left\{ F_{B \rightarrow K_0^*}^L(a_2) + \mathcal{M}_{B \rightarrow K_0^*}^L(C_2) \right\} \right. \\
& - V_{tb}V_{ts}^* \left\{ -F_{B \rightarrow \pi}^L(a_4 - \frac{1}{2}a_{10}) - F_{B \rightarrow \pi}^R(a_6 - \frac{1}{2}a_8) + F_{B \rightarrow K_0^*}^L(\frac{3}{2}a_9) + F_{B \rightarrow K_0^*}^R(\frac{3}{2}a_7) \right. \\
& - F_a^L(a_4 - \frac{1}{2}a_{10}) - F_a^R(a_6 - \frac{1}{2}a_8) \\
& - \mathcal{M}_{B \rightarrow \pi}^L(C_3 - \frac{1}{2}C_9) - \mathcal{M}_{B \rightarrow \pi}^R(C_5 - \frac{1}{2}C_7) + \mathcal{M}_{B \rightarrow K_0^*}^L(\frac{3}{2}C_{10}) + \mathcal{M}_{B \rightarrow K_0^*}^R(\frac{3}{2}C_8) \\
& \left. \left. - \mathcal{M}_a^L(C_3 - \frac{1}{2}C_9) - \mathcal{M}_a^R(C_5 - \frac{1}{2}C_7) \right\} \right]. \tag{40}
\end{aligned}$$

The isospin relation for the four channels holds exactly in these equations:

$$\sqrt{2}A(\bar{B}^0 \rightarrow \bar{K}_0^{*0}\pi^0) + A(\bar{B}^0 \rightarrow K_0^{*-}\pi^+) = \sqrt{2}A(B^- \rightarrow K_0^{*-}\pi^0) - A(B^- \rightarrow \bar{K}_0^{*0}\pi^-). \tag{42}$$

B. $B \rightarrow a_0 K$ decays

As mentioned above, the predicted branching fractions of $B \rightarrow a_0 K$, which overshoot the experimental limits, are regarded as an evidence to rule out scenario I in QCDF, thus it is important to see whether it is the same in the PQCD approach.

The Feynman diagrams for these decays are completely the same as the $B \rightarrow K_0^* \pi$ except that we should identify the $s\bar{q}$ and $q\bar{q}$ as K and a_0 rather than K_0^* and π , then each channel corresponds to the one in $B \rightarrow K_0^* \pi$. Their

factorization formulae can be derived from the corresponding channels directly. The K -emission and annihilation decay amplitudes of $B \rightarrow a_0 K$ can be obtained from $B \rightarrow K_0^* \pi$ by making the substitution:

$$\begin{aligned} \phi_{K_0^*} &\rightarrow \phi_K^A, \phi_{K_0^*}^S \rightarrow \phi_K^P, \phi_{K_0^*}^T \rightarrow \phi_K^T, \\ \phi_\pi^A &\rightarrow \phi_{a_0}, \phi_\pi^P \rightarrow -\phi_{a_0}^S, \phi_\pi^T \rightarrow -\phi_{a_0}^T. \end{aligned} \quad (43)$$

The a_0 -emission diagrams have only nonfactorizable contributions, the substitution for $(V - A)(V - A)$ operators is:

$$\phi_\pi^A \rightarrow \phi_{a_0}, \phi_\pi^P \rightarrow \phi_{a_0}^S, \phi_\pi^T \rightarrow \phi_{a_0}^T, \quad (44)$$

$$\phi_{K_0^*}^A \rightarrow \phi_K^A, \phi_{K_0^*}^S \rightarrow -\phi_K^P, \phi_{K_0^*}^T \rightarrow -\phi_K^T, \quad (45)$$

but for $(V - A)(V + A)$ operators,

$$\phi_\pi^A \rightarrow \phi_{a_0}, \phi_\pi^P \rightarrow \phi_{a_0}^S, \phi_\pi^T \rightarrow \phi_{a_0}^T, \quad (46)$$

$$\phi_{K_0^*}^A \rightarrow -\phi_K^A, \phi_{K_0^*}^S \rightarrow \phi_K^P, \phi_{K_0^*}^T \rightarrow \phi_K^T. \quad (47)$$

Compared with $B \rightarrow K_0^* \pi$, the features of $B \rightarrow a_0 K$ are:

- For the decays $\bar{B}^0 \rightarrow a_0^+ K^-$ and $B^- \rightarrow a_0^- \bar{K}^0$, the emitted particle is K , which can be produced through the axial-vector current without any suppression, thus the operator O_4 can give a large contribution to the emission factorizable amplitudes. But this term has a minus sign relative to O_6 , so the penguin operators cancel with each other sizably. The contribution from tree operators can be large due to the large Wilson coefficients a_1 in $B^- \rightarrow a_0^+ K^-$.
- In $B \rightarrow \bar{K}_0^{*0} \pi^-$, the emitted particle (\bar{K}_0^{*0}) is a scalar meson, the two hard spectator scattering diagrams (non-factorizable) can enhance each other due to the anti-symmetric twist-2 distribution amplitudes. But in $\bar{B}^0 \rightarrow a_0^+ K^-$ and $B^- \rightarrow a_0^- \bar{K}^0$, the emitted particle is a pseudoscalar, there are cancellations between the two hard spectator scattering diagrams. So the hard spectator scattering contribution is rather small.
- The annihilation diagrams of the four $B \rightarrow a_0 K$ channels are similar with each other, the dominant contributions are all from the $S \rightarrow P$ time-like form factor mediated by an $(S + P)$ density.
- $\bar{B}^0 \rightarrow a_0^0 \bar{K}^0$ and $B^- \rightarrow a_0^0 K^-$ are more complicated due to the appearance of the a_0 -emission diagrams. Because of the vanishing vector decay constant of a_0 , the factorizable emission diagrams are zero. For the nonfactorizable diagrams, the QCD penguin operators cancel for the neutral state of isospin triplet. The electroweak penguin operators have a small Wilson coefficients, thus the emission contributions in these channels are small. For the tree operators, although they are suppressed by the CKM matrix elements, the nonfactorizable emission diagrams can be enhanced for the large Wilson coefficients C_2 . So it is expected a large CP asymmetry in the decays $\bar{B}^0 \rightarrow a_0^0 \bar{K}^0$ and $B^- \rightarrow a_0^0 K^-$.

From the above discussion, we can see that the dominant contributions are from the annihilation diagrams and the diagrams with tree operators.

IV. RESULTS AND DISCUSSIONS

For numerical calculations, we have employed the parameters in Tab. I. For the B meson wave function, we adopt the Gaussian-type model [13] (we choose the shape parameter $\omega = 0.4$). As for the light-cone distribution amplitudes (LCDAs) of the pion and kaon, we use the results from QCD sum rules up to twist-3 [23]. Other parameters relevant to the scalar mesons have been given in the second section.

TABLE I: Input parameters used in the numerical calculation

Masses	$m_{K_0^*} = 1.412$ GeV,	$m_0^K = 1.7$ GeV,	$m_0^\pi = 1.4$ GeV
	$m_{a_0} = 0.98$ GeV	$M_B = 5.28$ GeV	
Decay constants	$f_B = 0.19$ GeV	$f_K = 0.16$ GeV	$f_\pi = 0.132$ GeV
Life Times	$\tau_{B^\pm} = 1.671 \times 10^{-12}$ s $\tau_{B^0} = 1.536 \times 10^{-12}$ s		
CKM	$V_{tb} = 0.9997$	$V_{ts} = -0.04,$	
	$V_{us} = 0.2196$	$V_{ub} = 0.00367e^{-i60^\circ}$	

TABLE II: Various decay amplitudes ($\times 10^{-2} \text{GeV}^3$) in decay $B^- \rightarrow \bar{K}_0^{*0} \pi^-$ and $B^- \rightarrow a_0^- \bar{K}^0$

	$F_e^L(a_4)$	$F_e^R(a_6)$	$\mathcal{M}_e^L(C_3) + M_e^R(C_5)$	$F_a^L(a_4) + F_a^R(a_6) + \mathcal{M}_a^L(C_3) + \mathcal{M}_a^R(C_5)$	$F_a^L(a_2) + \mathcal{M}_a^L(C_1)$
scenario I	0.98	-12	$0.78 + 1.2i$	$7.4 + 13.3i$	$8.8 - 11.8i$
scenario II	-1.4	17.9	$2.1 - 0.37i$	$-5.8 - 17.8i$	$-13.6 - 0.11i$
$B^- \rightarrow a_0^- \bar{K}^0$	9.3	-11.3	$0.09 - 0.74i$	$2.0 - 9.0i$	$8.6 + 1.2i$

A. The Branching Ratios and The CP Asymmetries

Using the parameters in the above, we give the numerical results for different amplitudes of $B^- \rightarrow \bar{K}_0^{*0} \pi^-$ in Table II. The numerical results confirm that the emission diagram of $(V - A)(V - A)$ operators $F_{B \rightarrow \pi}^L(a_4)$ indeed give small contributions because of the small vector current decay constant. The $(V - A)(V + A)$ operators give the dominant contribution $F_e^R(a_6)$. The opposite sign between scenario I and scenario II comes from the decay constant of the K_0^* meson. The non-factorizable contribution $\mathcal{M}_{B \rightarrow \pi}^L(C_3)$ is small due to the small Wilson coefficient. $\mathcal{M}_{B \rightarrow \pi}^R(C_5)$ is even smaller because of the cancellation between the two diagrams.

According to PQCD power counting, the annihilation diagrams are power suppressed, but the suppression is not so effective in some cases, such as when chiral enhancement existing. Usually there is a large imaginary part in the amplitudes of the annihilation diagrams, which is the source of strong phase in PQCD approach. The numerical results in Table II indicate that the annihilation diagrams in scenario I are more important than that in scenario II. There are also tree operators contributing to the annihilation diagrams $F_a^L(a_2) + \mathcal{M}_a^L(C_1)$, which are Cabibbo suppressed, but they are essential in direct CP violation.

Now it is straightforward to obtain the results for the CP -averaged branching ratio of $B^- \rightarrow \bar{K}_0^{*0} \pi^-$, which is given in Tab. III. Comparing the two scenarios, we find: the results from scenario II are twice as scenario I, the most important reason is the larger scalar decay constant in scenario II; secondly, the nonfactorizable diagrams are small, they only change the branching ratio slightly; the annihilation diagrams play an important role in both scenarios, it

TABLE III: Branching ratios for the decays $B \rightarrow K_0^* \pi$ and $B \rightarrow a_0 K$ (in units of 10^{-6}). The first theoretical error is from the decay constant of the scalar meson, the second and the third one is Gengebauer moments B_1 and B_3 , the uncertainty caused the CKM angle γ is very small which is not listed here. The experimental data listed here are the world average values by the Heavy Flavor Averaging Group (HFAG) [10].

Channel	scenario I	scenario II	exp.	Channel	scenario I	exp.
$B^- \rightarrow \bar{K}_0^{*0} \pi^-$	$20.7^{+4.3+0.8+1.8}_{-3.9-0.8-1.6}$	$47.6^{+11.3+3.7+6.9}_{-10.1-3.6-5.1}$	41.2 ± 4.2	$B^- \rightarrow \bar{K}^0 a_0^-$	$6.9^{+0.8+1.1+2.0}_{-0.7-1.1-1.7}$	< 3.9
$\bar{B}^0 \rightarrow K_0^{*-} \pi^+$	$20.0^{+4.2+0.8+1.6}_{-3.8-0.7-1.5}$	$43.0^{+10.2+3.1+7.0}_{-9.1-2.9-5.2}$	$46.6^{+5.6}_{-6.6}$	$\bar{B}^0 \rightarrow K^- a_0^+$	$9.7^{+1.1+1.6+2.7}_{-1.0-1.4-2.2}$	< 1.6
$\bar{B}^0 \rightarrow \bar{K}_0^{*0} \pi^0$	$10.0^{+2.1+0.4+1.0}_{-1.9-0.5-0.9}$	$18.4^{+4.4+1.5+4.0}_{-3.9-1.4-2.9}$	25.5 ± 9.9	$\bar{B}^0 \rightarrow \bar{K}^0 a_0^0$	$4.7^{+0.5+0.7+1.1}_{-0.5-0.8-1.1}$	< 7.8
$B^- \rightarrow K_0^{*-} \pi^0$	$11.3^{+2.4+0.4+0.7}_{-2.1-0.3-0.7}$	$28.8^{+6.8+1.9+3.2}_{-6.1-1.9-3.5}$	-	$B^- \rightarrow K^- a_0^0$	$3.5^{+0.4+0.4+1.0}_{-0.4-0.6-1.0}$	< 2.5

TABLE IV: Ratios of the branching fractions in $B \rightarrow K_0^* \pi$. For the experimental values, we only use the central values.

Ratios	isospin limit	Scenario II	Scenario I	Experiment
R_1	0.5	0.43	0.48	0.39
R_2	0.5	0.61	0.55	-
R_3	1.0	1.02	0.95	0.81

can enhance the branching ratios about 50% in scenario I, and about 30% in scenario II. The current experimental data [10] is also listed in Tab. III. The large branching ratio is consistent with the results in scenario II, so scenario II is more preferable than scenario I, this conclusion is consistent with [11]. But the difference with [11] is: we directly calculate the annihilation contribution in $B \rightarrow K_0^* \pi$, rather than fit the $B \rightarrow K_0^* \pi$ data and then use the $B \rightarrow a_0 K$ data to rule out scenario I.

The decay amplitudes for the $B^- \rightarrow a_0^- \bar{K}^0$ decay are also listed in table II, the results indicate that the emission diagrams almost cancelled out, as expected in section III. The branching ratio is dominated by the annihilation diagrams which is at the same level as the $B^- \rightarrow \bar{K}_0^{*0} \pi^-$, and the induced branching ratio is about twice larger than the experimental upper bound. The results also show that scenario I is not supported by the current experimental data.

In the above discussion, we concentrate on $B^- \rightarrow \bar{K}_0^{*0} \pi^-$ and $B \rightarrow a_0^- \bar{K}^0$. The dominant contribution in $B \rightarrow K_0^* \pi$ for other channels is the same with $B^- \rightarrow \bar{K}_0^{*0} \pi^-$ by isospin symmetry, except the contribution from the electro-weak penguin and the tree operators which can violate isospin symmetry. To explore the deviation of the isospin limit, it is convenient to define the parameters below:

$$\begin{aligned}
R_1 &= \frac{\mathcal{B}(\bar{B}^0 \rightarrow K_0^{*0} \pi^0)}{\mathcal{B}(\bar{B}^0 \rightarrow K_0^{*-} \pi^+)}, \\
R_2 &= \frac{\mathcal{B}(B^- \rightarrow K_0^{*-} \pi^0)}{\mathcal{B}(B^- \rightarrow K_0^{*0} \pi^-)}, \\
R_3 &= \frac{\tau(B^0) \mathcal{B}(B^- \rightarrow K_0^{*0} \pi^-)}{\tau(B^-) \mathcal{B}(\bar{B}^0 \rightarrow K_0^{*-} \pi^+)}.
\end{aligned} \tag{48}$$

For $B \rightarrow a_0 K$, the definition is the similar except $K_0^* \rightarrow K, \pi \rightarrow a_0$. These parameters are the ratios of the branching fractions, which should be less sensitive to many nonperturbative inputs than the branching fractions, thus it is more persuadable to test these parameters. In the isospin limit, if we ignore the CKM suppressed tree diagrams and electro-weak penguins, R_1, R_2 and R_3 should be equal to 0.5, 0.5 and 1.0. The deviations reflect the magnitude of the tree operators and the electro-weak penguins directly. Our results and the experimental data are given in table IV, where we use the central values in table III for the experiment data. In both scenarios, the deviations from isospin limit are not large, which shows that the QCD penguin are dominant in the branching ratios, both in emission diagrams and the annihilation diagrams. The three ratios for $B \rightarrow a_0 K$ decays are: $R_1 = 0.48, R_2 = 0.51, R_3 = 0.68$. There is a large deviation for the ratio R_3 , and the reason is the large tree contribution. So the large direct CP asymmetry for $B^0 \rightarrow a_0^- K^+$ is also expected.

The contribution from different effective operators shown in Eqs. (31-41) have been categorized to two groups according to the different CKM matrix elements:

$$\bar{A} = \frac{G_F}{\sqrt{2}} [V_{ub} V_{us}^* T - V_{tb} V_{ts}^* P], \tag{49}$$

where T/P denotes the amplitude which comes from the tree/penguin operators respectively. The charge conjugate channel decay amplitude is the same as Eq. (49) except the sign of the weak phase. The formula for the direct CP

TABLE V: Direct CP asymmetries (in units of %)

Channel	Scenario I	Scenario II	exp.	channels	A_{CP}
$B^- \rightarrow \bar{K}_0^{*0} \pi^-$	-1.5	-1.7	-5_{-8}^{+5}	$B^- \rightarrow \bar{K}^0 a_0^-$	4
$\bar{B}^0 \rightarrow K_0^{*-} \pi^+$	9.2	0.22	-7 ± 14	$\bar{B}^0 \rightarrow K^- a_0^+$	-70
$\bar{B}^0 \rightarrow \bar{K}_0^{*0} \pi^0$	-9.0	-6.8	-34 ± 19	$\bar{B}^0 \rightarrow \bar{K}^0 a_0^0$	-17
$B^- \rightarrow K_0^{*-} \pi^0$	16.0	3.5	-	$B^- \rightarrow K^- a_0^0$	-70

asymmetry reads:

$$A_{CP} = \frac{|\bar{A}|^2 - |A|^2}{|A|^2 - |A|^2} = \frac{2z \sin \gamma \sin \delta}{1 - 2z \cos \gamma \cos \delta + z^2}, \quad (50)$$

where $z = \left| \frac{V_{tb}V_{ts}^*}{V_{ub}V_{us}^*} \right| \left| \frac{P}{T} \right|$, δ is the relative strong phase between two groups of contributions. This equation indicates that the direct CP violation depends on the ratio of the tree and penguin contribution. The direct CP asymmetry is very small if the ratio is too large or too small, while the comparable tree and penguin contributions imply large direct CP asymmetries. For $B \rightarrow K_0^* \pi$, the penguin operators give the dominant contribution, but the tree operators suffer from the CKM suppression, so it is expected the direct CP asymmetry is small. We list our results in table V as well as the experimental data [10], where the results are consistent with the experiments in both scenarios. But in the decay $B^0 \rightarrow a_0 K$, as mentioned above, the emission penguin contribution cancels, while the tree operators are large, sizable direct CP asymmetries are predicted in these channels, especially in $\bar{B}^0 \rightarrow a_0^+ K^-$ and $B^- \rightarrow a_0^0 K^-$. In QCDF, the central values of direct CP asymmetries for all four channels are very small, but with large uncertainties for $B^- \rightarrow a_0^0 K^-$ and $\bar{B}^0 \rightarrow a_0^+ K^-$. Furthermore, we may expect the similar size of CP asymmetries in similar decays $B \rightarrow a_0(1450)K$.

B. The Theoretical Uncertainties

In the above calculation, the uncertainties from the decay constants can give sizable effects on the branching ratio, but not to the direct CP asymmetries. Furthermore, there are other sources of uncertainties:

- The twist-3 distribution amplitudes of the scalar mesons are taken as the asymptotic form for lack of more reasonable results from non-perturbative methods, which may give sizable uncertainties. These distribution amplitudes needs to be studied in future work [24].
- The Gegenbauer moments B_1 and B_3 for twist-2 LCDAs of K_0^* and a_0 have sizable uncertainties, which can lead to the theoretical errors. We include these uncertainties in the results and they can give about 20% ~ 30% uncertainties to the branching ratio.
- The uncertainties of the light pseudoscalar meson and B meson wave functions, the factorization scale, *et al.* have been studied extensively in [25]. The uncertainty from the factorization scale is within 10%. The major source of the uncertainty comes from the meson distribution amplitudes. The results can be varied by (10–30)% by changing the parameter in the wave functions.
- The sub-leading order contributions in PQCD approach have also been neglected in this calculation, but these corrections have been calculated in refs. [26] for $B \rightarrow \pi K, \pi\pi$, *etc.* These corrections can change the penguin dominated processes about 20% of the branching ratio of $B \rightarrow \pi K$. We may expect similar effect in $B \rightarrow K_0^* \pi$.
- The uncertainties of CKM matrix elements and the CKM phase angle can also affect the branching ratios and CP asymmetries. In the two kinds of decays considered in this paper, the decay amplitudes are the functions of

the CKM angle γ , whose value given in PDG06 is $\gamma = (63_{-12}^{+15})^\circ$ [27]. With the CKM angle γ varying at this area, we find that the error area is very small in $B \rightarrow K_0^* \pi$ decays in both scenarios. For the $B \rightarrow a_0 K$ decays, the error area is some larger, but within ten percent.

- The long distance re-scattering can also affect the branching ratios and CP asymmetries. This effect could be phenomenologically studied in the final-state interactions [28]. We need more data to determine whether it is necessary to include the re-scattering effect in $B \rightarrow SP$ decays.

V. SUMMARY

In this paper, we calculate the decay modes $B \rightarrow K_0^* \pi$ and $B \rightarrow a_0 K$ within perturbative QCD framework. For $B \rightarrow K_0^* \pi$, we perform our calculation in two scenarios of the scalar meson spectrum, our calculation indicates that: scenario II is more consistent with the experimental data than scenario I. We directly calculate the contribution from annihilation diagrams: it can enhance the branching ratios about 50% in scenario I, and about 30% in scenario II. Our predicted branching ratio of $B \rightarrow a_0 K$ in scenario I is larger than the experimental upper bound which may rule out the scenario I. We calculated the direct CP asymmetries and the isospin parameters in these decays, and we find that in $B \rightarrow K_0^* \pi$ (in both scenarios) the direct CP asymmetries are small, which are consistent with the present experiments; the deviation from the isospin limit is also small. There is large CP symmetries in $B \rightarrow a_0(980)K$ due to the relatively large tree contributions in scenario I. We expect similar CP asymmetries in $B \rightarrow a_0(1450)K$.

Acknowledgement

This work was partly supported by the National Science Foundation of China. We thank Y. Li, Y. M. Wang, M. Z. Yang and H. Zou for helpful discussions. C.D. Lü thanks A. Ali and G. Kramer for their hospitality during his visit at DESY.

-
- [1] For a review, see S. Spanier and N. A. Törnqvist, “Note on salar mesons” in Particle Data Group, Journal of Physics G **33**, 1 (2006); S.Godfrey and J. Napolitano, Rev. Mod. Phys. **71**,1411(1999); F. E. Close and N. A. Törnqvist, J. Phys. G **28**, R249(2002).
- [2] G.L. Jaffe, Phys. Rev. D**15**, 267(1977); *ibid*: **15**, 281(1977).
- [3] P. Minkowski and W. Ochs, Euro. Phys. J. **C9**, 283(1999).
- [4] Belle Collabaraion, K. Abe *et al.*, Phys. Rev. D**65**, 092005(2002).
- [5] Belle Collabaraion, A. Garmash *et al.*, Phys. Rev.D**71**, 092003(2005); Belle Collabaraion, A. Garmash *et al.*, arXiv: hep-ex/0505048.
- [6] Babar Collaboration, B. Aubert *et al.*, Phys. Rev. D**70**, 092001(2004); Phys. Rev. D**72**, 072003(2005); arXiv: hep-ex/0408032, hep-ex/0408073.
- [7] Belle Collaboration, K. Abe *et al.*, arXiv: hep-ex/0509047; Belle Collaboration, A. Bonder *et al.*, arXiv: hep-ex/0411004.
- [8] Belle Collaboration, K. Abe *et al.*, hep-ex/0509001.
- [9] Babar Collaboration, B. Aubert *et al.*, Phys. Rev. D**74**, 032003(2006); hep-ex/0607112.
- [10] Heavy Flavor Averaging Group, P. Chang, *et al.*, <http://www.slac.stanford.edu/xorg/hfag>.
- [11] H.-Y. Cheng, C.-K. Chua, K.-C. Yang, Phys. Rev. D**73**, 014017(2006).
- [12] A.V. Manohar and I.W. Stewart, arXiv: hep-ph/0607001.
- [13] Y. Y. Keum, H.-n. Li and A. I. Sanda, Phys. Lett. **B504**, 6(2001); Phys. Rev. D**63**, 054008 (2001); C.H. Chen, Y.Y. Keum and H.-n. Li, Phys. Rev. D**66**, 054013(2002).

- [14] C.-D. Lü, K. Ukai, M.-Z. Yang, Phys. Rev. **D63**, 074009 (2001); C. D. Lü and M. Z. Yang, Eur. Phys. J. **C23**, 275(2002).
- [15] C. D. Lü, K. Ukai, Eur. Phys. J. **C28**, 305 (2003); Y. Li, C. D. Lü, J. Phys. **G29**, 2115 (2003); High Energy Phys. Nucl. Phys. **27**, 1062(2003).
- [16] T.V. Brito, F.S. Navarra, M. Nielsen, and M.E. Fracco, Phys. Lett. **B608**, 69(2005); K. Maltman, Phys. Lett. **B462**, 14(1999); S. Narison, Nucl. Phys. Proc. Suppl. **86**, 242(2000); C.M. Shakin and H.S. Wang, Phys. Rev. **D63**, 074017(2001); D.S. Du, J.W. Li and M.Z. Yang, Phys. Lett.B **619**, 105(2005).
- [17] J. Botts and G. Sterman, Nucl. Phys. **B325**, 62 (1989).
- [18] H.N. Li, Prog. Part. Nucl. Phys. **51**, 85(2003).
- [19] For a review, see G. Buchalla, A.J. Buras, M.E. Lautenbacher, Rev. Mod. Phys. **68**, 1125(1996).
- [20] C.H. Chen, Y.Y. Keum and H.-n. Li, Phys. Rev. **D64**, 112002(2003).
- [21] W. Wang, Y.L. Shen, Y. Li and C.D. Lü, arXiv: hep-ph/0609082.
- [22] A. Ali, G. Kramer, C.D. Lü, Phys. Rev. **D58**, 094009 (1998)
- [23] V. M. Braun, I. E. Fliyakov, Z. Phys. **C48**, 239(1990); P. Ball, JHEP, **9901**, 010(1999).
- [24] C.D. Lü, Y.M. Wang and H. Zou, in progress.
- [25] T. Kurimoto, Phys. Rev. **D74**, 014027(2006).
- [26] H.N. Li, S. Mishima and A.I. Sanda, Phys. Rev. **D72**, 114005(2005); H.N. Li and S. Mishima, *ibid*: **73**,114014(2006); arXiv: hep-ph/0608277.
- [27] Particle data group, Journal of Physics G **33**, 1 (2006).
- [28] H.Y. Cheng, C.K. Chua and A. Soni, Phys. Rev. **D71**, 014030(2005); C.D. Lü, Y.L. Shen and W. Wang, Phys. Rev. **D73**, 034005(2006).